

# Padé schemes with Richardson extrapolation for the sine-Gordon equation

Francisca Martin-Vergara, Francisco Rus, Francisco R. Villatoro\*

*<sup>a</sup>Escuela de Ingenierías Industriales, Dept. de Lenguajes y Ciencias de la Computación, Universidad de Málaga, 29071 Málaga, Spain*

---

## Abstract

Four novel implicit finite difference methods with  $(q + s)$ -th order in space based on Padé approximations have been analyzed and developed for the sine-Gordon equation. Specifically,  $(0, 4)$ ,  $(2, 2)$ ,  $(2, 4)$ , and  $(4, 4)$  Padé methods. All of them share the treatment for the nonlinearity and integration in time, specifically, the one that results in an energy-conserving  $(0, 2)$  Padé scheme. The five methods have been developed with and without Richardson extrapolation in time. All the methods are linearly, unconditionally stable. A comparison among them for both the kink–antikink and breather solutions in terms of global error, computational cost and energy conservation is presented. Our results indicate that the  $(0, 4)$  and  $(4, 4)$  Padé methods without Richardson extrapolation are the most cost-effective ones for small and large global error, respectively; and the  $(4, 4)$  Padé methods in all the cases when Richardson extrapolation is used.

*Keywords:* Sine-Gordon equation, Padé numerical methods, Implicit time integration, Richardson extrapolation

---

## 1. Introduction

The one-dimensional sine-Gordon equation (sGE) has been used for modeling a large amount of physical systems in classical field theory. To mention just a few, it models the propagation of magnetic flux in large Josephson junctions, dislocations in crystals, nonlinear spin waves in superfluids, or waves in ferro-  
5 magnetic and anti-ferromagnetic materials, among others [1, 2, 3]. The great advantage of the sGE as a model in physics is its exact solvability [4, 5]. The general solution for its initial-value problem can be obtained by using the inverse scattering method, a kind of nonlinear Fourier method [6, 7]. The numerical  
10 study of the sGE with small perturbations still attract the attention of mathematicians and physicists [3], including new applications, like the propagation of nonlinear electromagnetic waves in graphene superlattices [8].

---

\*Corresponding author: Tel.: +34-951952388; fax: +34-951952542.

*Email addresses:* [fmarter@uma.es](mailto:fmarter@uma.es) (Francisca Martin-Vergara), [fdrus@uma.es](mailto:fdrus@uma.es) (Francisco Rus), [frvillatoro@uma.es](mailto:frvillatoro@uma.es) (Francisco R. Villatoro)

Guo Ben-Yu et al. [9] developed an implicit, energy-conserving, leapfrog finite difference scheme for the Klein–Gordon equation. This method was inspired in the explicit one developed by Strauss and Vázquez [10], first used for the sGE in Ref. [11]. These methods are energy-conserving and second-order in both space and time.

Finite difference schemes based on  $(q, s)$  Padé approximants, with  $(q + s)$ -th order in space, are also referred to as compact operator methods.  $(0, 2)$ ,  $(1, 1)$ , and  $(1, 2)$  Padé methods were developed by Bratsos and Twizell [12]; a  $(2, 2)$  scheme by Duncan [13], applied to the sGE in Bratsos [14]; and a  $(2, 4)$  one by Sari and Güarslan [15]. A comparison of some Padé methods shows that the high-order ones are more efficient for high accuracy [13]. In fact, fourth-order Padé methods were used for the two-dimensional sGE in Refs. [16, 17, 18]. All these Padé methods use the nonlinearity treatment of the finite difference scheme developed by Perring and Skyrme [19] (the first numerical method for the sGE until these authors’ knowledge).

Recently, we have developed  $(0, 4)$ ,  $(2, 2)$ ,  $(2, 4)$ , and  $(4, 4)$  Padé methods for the sGE using the nonlinearity treatment developed by Strauss and Vázquez [10]; our results show that the most cost-effective ones are those of higher order, being the spatial order of accuracy more relevant for accuracy than the energy conservation property, even in long-time integrations [20]. Similar conclusions have been obtained for other schemes in older studies [13, 21, 22].

Richardson extrapolation (RE) can be used to increase the order of accuracy of a numerical method [23]. This technique could be applied in both space and time [24, 25], but in this paper will be applied only in time. The successful application of RE requires the knowledge of the order of accuracy of the numerical scheme calculated by means of an asymptotic expansion of the truncation error. In practice, codes solving partial differential equations may not achieve the theoretical order of accuracy. For the sGE, the best results have been obtained by applying only one level of extrapolation in time [26, 27]. Let us also emphasize that in long-time integrations the use of RE requires restarting to cope with phase errors in velocity [28, 29].

The goal of this paper is the development and comparison of new Padé methods with the nonlinearity treatment developed by Guo Ben-Yu et al. [9], with and without Richardson extrapolation. The contents of this paper are as follows. Section 2 presents five numerical Padé approximation schemes for the sGE; their local truncation error terms are given in Subsection 2.1; their linear stability analysis is in Subsection 2.2; and the implementation details, including the application of RE, the Newton’s iterative method and the avoidance of catastrophic cancellations in the nonlinearity are exposed in Subsection 2.3. A detailed comparison of the five methods with and without RE is presented in Section 3, for the kink-antikink solution in Subsection 3.1, and for the breather one in Subsection 3.2. Finally, the last section summarizes the main conclusions.

55 **2. Numerical schemes**

The non-dimensional form for the initial-value problem of the sGE is written as

$$\frac{\partial^2 u}{\partial t^2} - \frac{\partial^2 u}{\partial x^2} + \frac{dF(u)}{du} = 0, \quad x \in \mathbb{R}, \quad t \geq 0, \quad (1)$$

60 
$$u(x, 0) = u_0(x), \quad \frac{\partial u}{\partial t}(x, 0) = u_1(x), \quad (2)$$

where  $u(x, t)$  denotes the amplitude of the solution,  $x$  is the spatial coordinate,  $t$  is time, and  $F(u) = 1 - \cos(u)$  is the potential energy, with  $dF(u)/du = \sin(u)$ . It is well-known that the sGE is integrable with an infinite set of conservation laws. The momentum and energy of the solutions can be used to assess the accuracy of the numerical solution; they are given by

65 
$$P(t) = - \int_{-\infty}^{\infty} \left( \frac{\partial u}{\partial t} \right) \left( \frac{\partial u}{\partial x} \right) dx = P(0), \quad (3)$$

and

$$E(t) = \int_{-\infty}^{\infty} \left( \frac{1}{2} \left( \frac{\partial u}{\partial t} \right)^2 + \frac{1}{2} \left( \frac{\partial u}{\partial x} \right)^2 + F(u) \right) dx = E(0), \quad (4)$$

respectively. The speed of the kinks (antikinks) of the sGE can be calculated by using  $v(t) = P(t)/E(t)$ ; note that  $|P(t)| \leq E(t)$ , since  $F(u)$  is positive definite.

Let us consider the general Padé numerical method given by

$$\mathcal{A}_i(\mathbf{E}) \frac{U_m^{n+1} - 2U_m^n + U_m^{n-1}}{\Delta t^2} - \mathcal{B}_i(\mathbf{E}) \frac{(U_m^{n+1} + U_m^{n-1})}{2} + \mathcal{A}_i(\mathbf{E}) H(U_m^{n+1}) = 0, \quad (5)$$

with

$$H(U_m^{n+1}) \equiv \frac{F(U_m^{n+1}) - F(U_m^{n-1})}{U_m^{n+1} - U_m^{n-1}}, \quad (6)$$

75 where  $\mathcal{A}_i^{-1}(\mathbf{E}) \mathcal{B}_i(\mathbf{E}) u_m^n$  is a Padé approximant for the second-order spatial derivative of  $u(x_m, t^n)$ , with  $\mathbf{E}$  being the shift operator, i.e.,  $\mathbf{E} U_m^n = U_{m+1}^n$ ,  $U_m^n \approx u(x_m, t^n) = u_m^n$ , with  $x_m = m \Delta x$ ,  $m \in \mathbb{Z}$ , with  $\Delta x$  as the grid size, and  $t^n = n \Delta t$ ,  $n \in \mathbb{N}$ , with  $\Delta t$  as the time step. Hereon, for the numerical solution of the initial-value problem of Eq. (1), periodic boundary conditions are used in the finite interval  $x \in (-L/2, L/2]$ , with  $x_m = -L/2 + m \Delta x$ ,  $m = 1, 2, \dots, M$ , and  $\Delta x = L/M$  (note that  $x_0 \equiv x_M$ ), and a finite time interval  $t \in [0, T]$ , with  $t^n = n \Delta t$ ,  $n = 0, 1, \dots, N$ , and  $\Delta t = T/N$ .

**Method 1.** The finite difference method developed by Guo Ben-Yu *et al.* [9] is interpreted as a (0,2)-Padé method by using

85 
$$\mathcal{A}_1(\mathbf{E}) = \mathcal{I},$$

$$\mathcal{B}_1(\mathbf{E}) = \frac{\mathbf{E}^{-1} - 2 + \mathbf{E}^1}{\Delta x^2},$$

where  $\mathcal{I}$  is the identity operator. Method 1 is second-order accurate in space ( $p_1 = 2$ ) since

$$\frac{\mathcal{B}_1(\mathbf{E})}{\mathcal{A}_1(\mathbf{E})} u(x_m, t^n) = \frac{\partial^2 u}{\partial x^2} + \frac{\Delta x^2}{12} \frac{\partial^4 u}{\partial x^4} + \mathcal{O}(\Delta x^4).$$

**Method 2.** A novel (0,4)-Padé method with a fourth-order discretization of the spatial derivatives given by

$$\mathcal{A}_2(\mathbf{E}) = \mathcal{I},$$

$$\mathcal{B}_2(\mathbf{E}) = \frac{-\mathbf{E}^{-2} + 16 \mathbf{E}^{-1} - 30 + 16 \mathbf{E}^1 - \mathbf{E}^2}{12 \Delta x^2}.$$

By using Taylor series expansion, the Padé operator yields

$$\frac{\mathcal{B}_2(\mathbf{E})}{\mathcal{A}_2(\mathbf{E})} u(x_m, t^n) = \frac{\partial^2 u}{\partial x^2} - \frac{\Delta x^4}{90} \frac{\partial^6 u}{\partial x^6} + \mathcal{O}(\Delta x^6).$$

**Method 3.** A novel (2,2)-Padé approximation written as

$$\mathcal{A}_3(\mathbf{E}) = \frac{\mathbf{E}^{-1} + 10 + \mathbf{E}^1}{12},$$

$$\mathcal{B}_3(\mathbf{E}) = \frac{\mathbf{E}^{-1} - 2 + \mathbf{E}^1}{\Delta x^2},$$

which approximates the second-order derivative up to the fourth-order, as shown by Taylor series expansion,

$$\frac{\mathcal{B}_3(\mathbf{E})}{\mathcal{A}_3(\mathbf{E})} u(x_m, t^n) = \frac{\partial^2 u}{\partial x^2} - \frac{\Delta x^4}{240} \frac{\partial^6 u}{\partial x^6} + \mathcal{O}(\Delta x^6).$$

**Method 4.** A novel, sixth-order accurate in space, (2,4)-Padé approximation given by

$$\mathcal{A}_4(\mathbf{E}) = \frac{2 \mathbf{E}^{-1} + 11 + 2 \mathbf{E}^1}{3},$$

$$\mathcal{B}_4(\mathbf{E}) = \frac{\mathbf{E}^{-2} + 16 \mathbf{E}^{-1} - 34 + 16 \mathbf{E}^1 + \mathbf{E}^2}{4 \Delta x^2},$$

which can be easily checked by Taylor series expansion yielding

$$\frac{\mathcal{B}_4(\mathbf{E})}{\mathcal{A}_4(\mathbf{E})} u(x_m, t^n) = \frac{\partial^2 u}{\partial x^2} + \frac{23 \Delta x^6}{75600} \frac{\partial^8 u}{\partial x^8} + \mathcal{O}(\Delta x^8).$$

**Method 5.** A novel eighth-order accurate (4,4)-Padé approximation written as

$$\mathcal{A}_5(\mathbf{E}) = \frac{23 \mathbf{E}^{-2} + 688 \mathbf{E}^{-1} + 2358 + 688 \mathbf{E}^1 + 23 \mathbf{E}^2}{15},$$

115

$$\mathcal{B}_5(\mathbb{E}) = \frac{31 \mathbb{E}^{-2} + 128 \mathbb{E}^{-1} - 318 + 128 \mathbb{E}^1 + 31 \mathbb{E}^{-2}}{\Delta x^2},$$

whose accuracy can be verified by Taylor series expansion resulting in

$$\frac{\mathcal{B}_5(\mathbb{E})}{\mathcal{A}_5(\mathbb{E})} u(x_m, t^n) = \frac{\partial^2 u}{\partial x^2} - \frac{79 \Delta x^8}{4762800} \frac{\partial^{10} u}{\partial x^{10}} + \mathcal{O}(\Delta x^{10}).$$

The existence, uniqueness, and regularity of the solutions of the initial-boundary value problem for the sGE is widely known in the literature. For example, Theorem B.5 in Ref. [30, Appendix B] states that for  $u_0(x) \in L^p(\mathbb{R})$ ,  $\partial u_0(x)/\partial x \in L^p(\mathbb{R})$ , and  $u_1(x) \in L^p(\mathbb{R})$ , the unique weak solution of the sGE for  $t \in [0, T]$  is  $u(x, t) \in L^p(\mathbb{R}) \times L^\infty[0, T]$ . Hence, for a regular enough initial condition, the classical solution achieves the same regularity, and there is no problem with the consistency in both space and time for Methods 1–5.

### 2.1. Local truncation error

Let us determine the local truncation error terms  $\mathcal{L}_i(u)$  of Method 1–5. By using Taylor series expansion, after the substitution of  $U_m^n$  by the exact solution  $u(x_m, t^n)$  in Eq. (5) for the  $i$ -th method, results in

$$\mathcal{M}_i(u) \equiv \mathcal{G}(u) + \mathcal{L}_i(u) = 0, \quad (7)$$

where  $\mathcal{G}(u)$  is the sine-Gordon equation, cf.

$$\mathcal{G}(u) \equiv \frac{\partial^2 u}{\partial t^2} - \frac{\partial^2 u}{\partial x^2} + \sin(u),$$

and the local truncation error is

$$\mathcal{L}_i(u) = \mathcal{T}(u) \Delta t^2 + \mathcal{S}_i(u) \Delta x^{p_i} + \text{h.o.t.}, \quad (8)$$

where h.o.t. corresponds to the higher-order terms depending on  $u$  and its partial derivatives,  $p_i$  is spatial order of accuracy of the  $i$ -th method, and

$$\begin{aligned} \mathcal{T}(u) = & -\frac{1}{6} \sin(u) \left( \frac{\partial u}{\partial t} \right)^2 + \frac{1}{2} \cos(u) \frac{\partial^2 u}{\partial t^2} + \frac{1}{12} \frac{\partial^4 u}{\partial t^4} \\ & - \frac{1}{2} \sin(u) \left( \frac{\partial u}{\partial x} \right)^2 + \frac{1}{2} \cos(u) \frac{\partial^2 u}{\partial x^2} - \frac{1}{2} \frac{\partial^4 u}{\partial x^4}. \end{aligned}$$

**Method 1.** The local truncation error for Method 1 is given by

$$\mathcal{L}_1(u) = \mathcal{T}(u) \Delta t^2 - \frac{\Delta x^2}{12} \frac{\partial^4 u}{\partial x^4} + \text{h.o.t.} \quad (9)$$

**Method 2.** The local truncation error for Method 2 can be written as

$$\mathcal{L}_2(u) = \mathcal{T}(u) \Delta t^2 + \frac{\Delta x^4}{90} \frac{\partial^6 u}{\partial x^6} + \text{h.o.t.} \quad (10)$$

**Method 3.** For this method, the calculation of the local truncation error yields

$$\mathcal{L}_3(u) = \mathcal{T}(u) \Delta t^2 + \frac{\Delta x^4}{240} \frac{\partial^6 u}{\partial x^6} + \text{h.o.t.} \quad (11)$$

**Method 4.** In this case, the local error is

$$\mathcal{L}_4(u) = \mathcal{T}(u) \Delta t^2 - \frac{23 \Delta x^6}{75600} \frac{\partial^8 u}{\partial x^8} + \text{h.o.t.} \quad (12)$$

**Method 5.** The local error for Method 5 is given by

$$\mathcal{L}_5(u) = \mathcal{T}(u) \Delta t^2 + \frac{79 \Delta x^8}{4762800} \frac{\partial^{10} u}{\partial x^{10}} + \text{h.o.t.} \quad (13)$$

Note that the  $C^\infty$  regularity of the solutions of the initial-boundary value problem for the sGE for a  $C^\infty$  initial condition ensures that the truncation error terms for Methods 1–5 are properly defined.

## 2.2. Stability analysis

The linear stability of Methods 1–5 can be studied by using the von Neumann analysis of Eq. (5) with  $F \equiv 0$ . Let us substitute in Eq. (5) the Fourier expansion of  $Z_m^n = U_m^n - U_m^{n*} = e^{im\beta\Delta x} \xi^n$ , where  $U_m^{n*}$  is a reference solution,  $i = \sqrt{-1}$ ,  $\beta$  is the spatial frequency, and  $\xi$  is the amplification factor. After cancelling common factors the resulting polynomial equation for  $\xi$  is given by

$$p_i(\xi) = A_i \xi^2 - 2 B_i \xi + A_i = 0, \quad (14)$$

whose two roots  $\xi_1$  and  $\xi_2$  have modulus smaller than or equal to unity for every  $\xi$  if and only if  $|B_i| \leq A_i$ , i.e.,  $-A_i \leq B_i \leq A_i$ . These two inequalities yield necessary condition for linear stability on both  $\Delta x$  and  $\Delta t$ . For simplicity, let us use  $r = \Delta t / \Delta x$ , and  $\omega = \beta \Delta x / 2$ .

**Method 1.** The stability polynomial (14) for the Guo Ben-Yu *et al.* [9] method has coefficients

$$A_1 = B_1 + 2 r^2 \sin^2(\omega), \quad B_1 = 1.$$

**Method 2.** The stability polynomial (14) for this method is given by

$$A_2 = B_2 + \frac{8}{3} r^2 \sin^2(\omega) - \frac{1}{6} r^2 \sin^2(2\omega), \quad B_2 = 1.$$

**Method 3.** This method has a stability polynomial (14) with coefficients

$$A_3 = B_3 + 2 r^2 \sin^2(\omega), \quad B_3 = 1 - \frac{1}{3} \sin^2(\omega).$$

**Method 4.** The stability polynomial (14) of this method can be written as

$$A_4 = B_4 + 8 r^2 \sin^2(\omega) + \frac{1}{2} r^2 \sin^2(2\omega),$$

$$B_4 = 5 - \frac{8}{3} \sin^2(\omega).$$

175 **Method 5.** The stability polynomial (14) of this method yields

$$A_5 = B_5 + 256 r^2 \sin^2(\omega) + 62 r^2 \sin^2(2\omega),$$

$$B_5 = 252 - \frac{2752}{15} \sin^2(\omega) - \frac{92}{15} \sin^2(2\omega).$$

180 The stability conditions for the five methods  $-A_i \leq B_i$ , and  $B_i \leq A_i$  are always true, since  $B_i \geq 0$ , and  $A_i - B_i \geq 0$ , in all the cases. Hence, the five methods are linearly, unconditionally stable.

Method 1 is nonlinearly stable since it exactly conserves a positive definite, discrete analogue of the energy (4), concretely [9]

$$185 \quad E^n = \Delta x \sum_m \left[ \frac{1}{2} \left( \frac{U_m^{n+1} - U_m^n}{\Delta t} \right)^2 + \left( \frac{U_{m+1}^{n+1} - U_m^{n+1}}{2 \Delta x} \right)^2 + \left( \frac{U_{m+1}^n - U_m^n}{2 \Delta x} \right)^2 \right] \\ + \Delta x \sum_m \left[ \frac{F(U_m^{n+1}) + F(U_m^n)}{2} \right]. \quad (15)$$

For a fair comparison of the five methods, the same discrete energy (15) will be used for all the methods.

Let us also use a discrete analogue of the momentum (3) given by [9]

$$P^n = -\Delta x \sum_m \left[ \left( \frac{U_m^{n+1} - U_m^n}{\Delta t} \right) \left( \frac{U_{m+1}^n - U_{m-1}^n}{2 \Delta x} \right) \right]. \quad (16)$$

190 Thanks to the Lax equivalence theorem, Methods 1–5 are convergent since they are consistent and linearly stable. Moreover, Method 1 is also nonlinearly stable, so in long-time integrations it is expected to behave better than the other four methods; however, in practice, this behaviour should be further explored.

### 2.3. Richardson extrapolation and implementation

195 In order to increase the order of Methods 1–5 from their second-order up to the fourth-order of accuracy in time, Richardson extrapolation can be used. Let us apply only one level of Richardson extrapolation by using

$$U_m^{n+1} = \frac{4 U_m^{n+1,(\Delta t/2)} - U_m^{n+1,(\Delta t)}}{3}, \quad (17)$$

200 where  $U_m^{n+1,(\Delta t/2)}$  and  $U_m^{n+1,(\Delta t)}$  are the second-order approximations in time to  $u(x_m, t^{n+1})$  calculated with timesteps  $\Delta t/2$  and  $\Delta t$ , respectively, and  $U_m^{n+1}$  is its fourth-order extrapolation in time.

Methods 1–5 are implicit, hence a nonlinear equation should be solved for the calculation of  $U_m^{n+1}$  from  $U_m^n$  and  $U_m^{n-1}$  in Eq. (5). Let us use Newton’s iterative method given by

$$\begin{aligned}
205 \quad \mathcal{A}_i(\mathbf{E}) \left( U_m^{(k+1)} - 2U_m^n + U_m^{n-1} \right) - \Delta t^2 \mathcal{B}_i(\mathbf{E}) \frac{(U_m^{(k+1)} + U_m^{n-1})}{2} \\
+ \Delta t^2 \mathcal{A}_i(\mathbf{E}) \left( H(U_m^{(k)}) + H_u(U_m^{(k)}) (U_m^{(k+1)} - U_m^{(k)}) \right) = 0, \quad (18)
\end{aligned}$$

with

$$H_u(U_m^{(k)}) \equiv \frac{F_u(U_m^{(k)}) (U_m^{(k)} - U_m^{n-1}) - (F(U_m^{(k)}) - F(U_m^{n-1}))}{(U_m^{(k)} - U_m^{n-1})^2}. \quad (19)$$

Our stopping test for Newton’s iteration convergence is based on the relative error using the infinite norm, i.e.,  $\|U_m^{(k+1)} - U_m^{(k)}\|_\infty \leq \text{ToI}_{\text{rel}} \|U_m^{(k+1)}\|_\infty$ , with  $\|U_m^{(k)}\|_\infty = \max_m |U_m^{(k)}|$ , and  $\text{ToI}_{\text{rel}}$  being a small enough relative tolerance.

In the numerical evaluation of Eqs. (6) and (19) there exists catastrophic cancellations when  $|U_m^{(k)} - U_m^{n-1}| \ll 1$ . For the sGE, they can be avoided by rearranging the expression of  $H(U)$  by means of the exact formula [31, 32, 33]

$$215 \quad H(U) = \frac{\cos(U) - \cos(U_m^{n-1})}{U - U_m^{n-1}} = \frac{2 \sin((U + U_m^{n-1})/2) \sin((U - U_m^{n-1})/2)}{U - U_m^{n-1}},$$

and that of  $H_u(U)$  by means of

$$H_u(U) = \frac{\sin(U)}{U - U_m^{n-1}} - \frac{2 \sin((U + U_m^{n-1})/2) \sin((U - U_m^{n-1})/2)}{(U - U_m^{n-1})^2}.$$

Let us highlight that, although round-off errors are reduced after the application of these rearrangements, the discrete energy-conservation property of Method 1 can be affected by its use; the corresponding penalty grows as the numbers of points where these rearrangements do.

### 3. Numerical results

Let us summarize the main results for the comparison of Methods 1–5 both with and without RE for sGE, obtained after a large set of simulations for the kink–antikink and breather solutions. The five methods are compared in terms of error, energy conservation, and computational cost. Subsection 3.1 shows the results for a kink–antikink solution and Subsection 3.2 for the breather solution.

#### 3.1. Kink–antikink

The analytical solution of the sGE for a kink–antikink collision is given by

$$230 \quad u_{ka}(x, t) = 4 \tan^{-1} \frac{\sinh(v(t-10)/r_-)}{v \cosh(x/r_-)}, \quad (20)$$

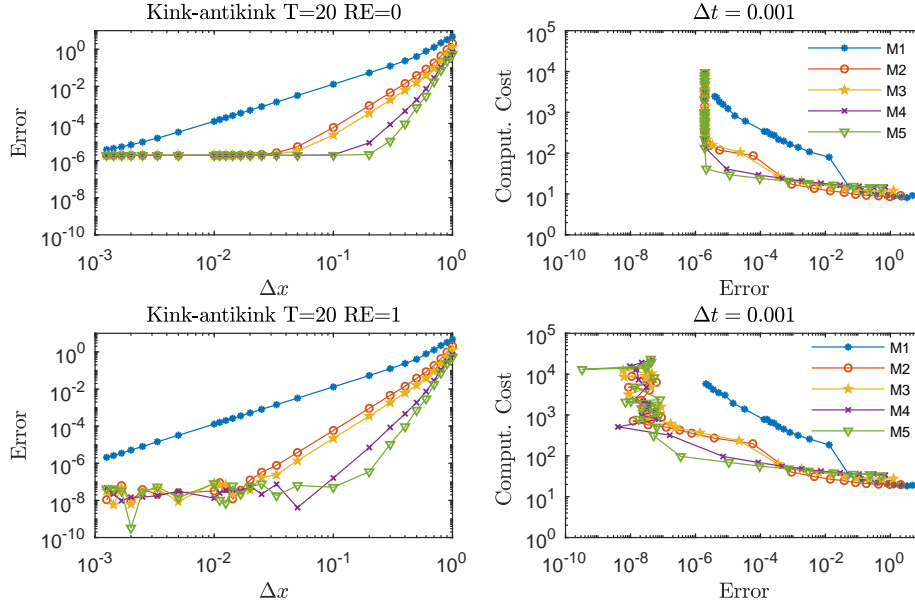


Figure 1: Numerical error (left plots) and computational cost (right plots) with (bottom plots) and without (top plots) RE for the kink-antikink solution with  $T = 20$  and  $\Delta t = 0.001$  as a function of  $\Delta x \in [1/800, 1/700, \dots, 1/100, 1/90, 1/80, \dots, 1/10, 2/10, 3/10, \dots, 1]$  for Methods 1–5.

where  $r_- = \sqrt{1 - v^2}$ . Methods 1–5 with the initial conditions (2) approximated by means of  $U_m^0 = u_{ka}(x_m, 0)$ , and  $U_m^{-1} = u_{ka}(x_m, -\Delta t)$ , with  $v = 1/2$ , yield the numerical solution  $U_m^n$  for  $n = 1, 2, \dots, N$ . Let us present results as function of  $\Delta t$  and  $\Delta x$ , with  $T = 20$ ,  $L = 50$ , and  $\text{ToI}_{\text{rel}} = 10^{-14}$ .

235 Table 1 shows a linear fitting of the logarithm of the numerical error versus the logarithm of the grid size for Methods 1–5 without and with RE, for  $\Delta t = 0.001$ ,  $T = 20$ , and  $L = 50$  with several values of  $\Delta x \in [1/800, 1]$ . This table validates the spatial order of Methods 1–5 since the results are in good agreement with the theoretical orders of accuracy, cf. 2, 4, 4, 6, and 8, respectively.

240 Figure 1 (left plots) shows the numerical error  $\|U_m^N - u_{ka}(x_m, 20)\|_\infty$  for

Table 1: The numerical order of accuracy in space of Methods 1–5 obtained by linear fitting of the logarithm of the error versus the logarithm of the grid size (fitted only for  $\Delta x$  such that the error in time is smaller than the error in space). The results in this table have  $L = 50$ ,  $\Delta t = 0.001$ , and  $T = 20$ .

	Method 1	Method 2	Method 3	Method 4	Method 5
Fit for $\Delta x \geq$	1/800	1/30	1/30	1/10	1/5
Without RE	2.06	3.98	3.92	5.83	8.14
With RE	2.12	4.22	4.37	6.66	8.93

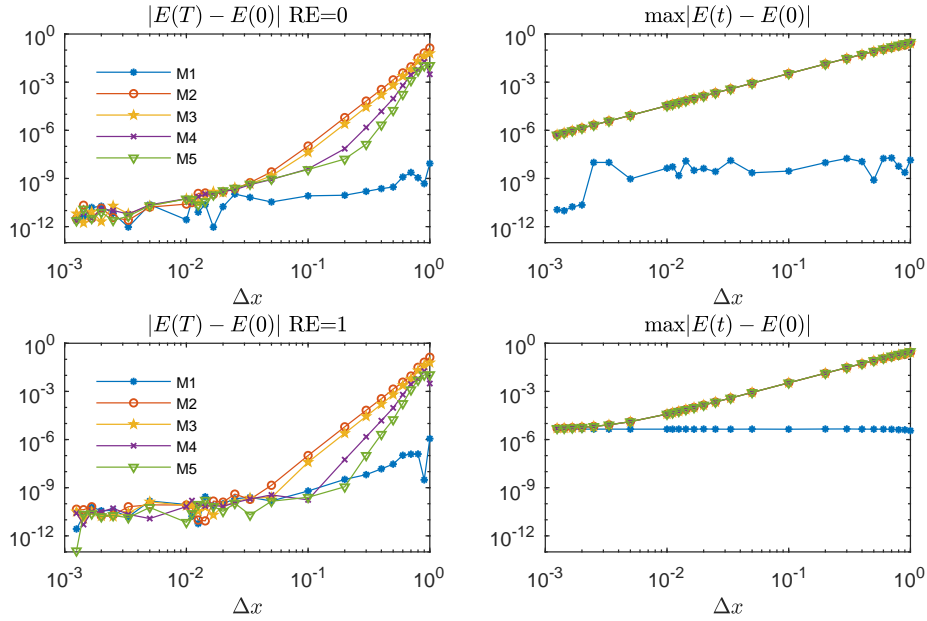


Figure 2: Numerical error  $|E^N - E^0|$  (left plots) and  $\|E^n - E^0\|_\infty$  (right plots) of the discrete energy, with (bottom plots) and without (top plots) RE, for the kink-antikink solution with the same parameters as Fig. 1.

Methods 1–5 with RE (left bottom plot) and without RE (left top plot), using  $\Delta t = 0.001$  and  $\Delta x \in [1/800, 1/700, \dots, 1/100, 1/90, 1/80, \dots, 1/10, 2/10, 3/10, \dots, 1]$ . In both cases the error decreases as  $\Delta x$  does until the contribution of the timestep dominates that of the grid size; without RE the error in time is about  $2 \times 10^{-6}$ , and with RE it is in the band of  $10^{-7}$  and  $10^{-8}$ .

Figure 1 (right plots) shows the computational cost, estimated by using the run-time in seconds, for Methods 1–5 with (bottom right plot) and without (top right plot) RE as a function of the numerical error; note that  $\Delta x > \Delta t = 0.001$  is used. It is observed that without Richardson extrapolation Method 2 is the most efficient one for errors larger than  $10^{-3}$  in terms of computational cost; for errors smaller than  $10^{-3}$ , Method 5 is the most cost-effective one, being about tens of times more efficient than Method 1. In the case of using RE the trends are similar, but with a higher cost and reaching an smaller error, down to the band between  $10^{-7}$  and  $10^{-8}$ , instead of  $10^{-6}$  attainable without RE.

Figure 2 shows the energy conservation of Methods 1–5 by using the discrete energy (15), exactly conserved by Method 1, in order to make a fair comparison of the energy conservation properties among all the methods; specifically, this figure shows the value of  $|E^N - E^0|$  (left plots) and  $\|E^n - E^0\|_\infty$  (right plots), without (top plots) and with (bottom plots) RE, for Methods 1–5 with  $T = 20$  and  $\Delta t = 0.001$  as a function of  $\Delta x \in [1/800, 1]$ . For Method 1, the left top plot

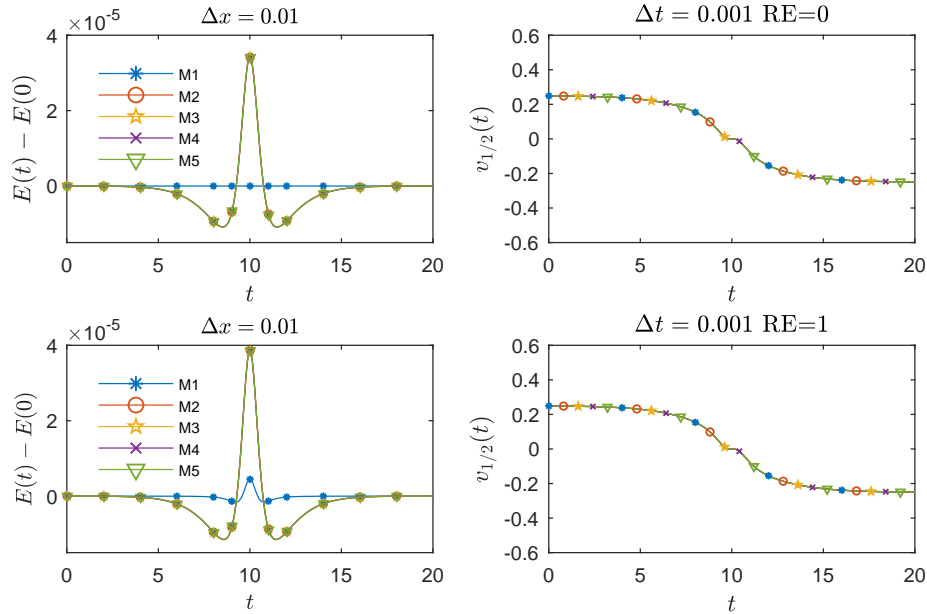


Figure 3: Evolution in time of the energy  $E^n - E^0$  (left plots) and of the speed  $V(t^n)$  (right plots), with (bottom plots) and without (top plots) RE, for the kink-antikink solution with  $T = 20$ ,  $\Delta t = 0.001$ , and  $\Delta x = 0.01$ , for Methods 1–5.

in Fig. 2 confirms that the discrete energy (15) is exactly conserved without RE. However, it is not exactly conserved with RE, as shown in the left bottom plot in Fig. 2; although the extrapolated solution is obtained by a linear combination of two solutions both conserving the discrete energy, this property is lost due to the nonlinearity in Eq. (15). Methods 2–5 without RE (left top plot in Fig. 2) only show good conservation properties for  $\Delta x \leq 1/30$ ; but for  $\Delta x > 1/30$  the error in the energy increases as the grid size does, with a higher slope for higher-order methods; but when using RE (left bottom plot), the higher time accuracy of the methods results in good conservation properties when  $\Delta x \leq 1/5$  for Method 5, when  $\Delta x \leq 1/10$  for Method 4, and when  $\Delta x \leq 1/20$  for Methods 2–3.

Figure 2 (right plots) shows that the maximum error in the energy is nearly constant for Method 1 with (bottom plots) and without (top plots) RE. For Methods 2–5 its value decreases with  $\Delta x$ , being equal for all the methods independently of the spatial order of each method. The loss of conservation of Method 1 with RE is observed in the bottom right plot of Fig. 2, where the maximum error in energy is approximately equal to  $4.4 \times 10^{-6}$ , being independent of  $\Delta x$ , and equal to that of Methods 2–5 for the smallest values of  $\Delta x$ .

In order to understand the results observed in the right plots of Fig. 2, the maximum error in the discrete energy is shown in Fig. 3 (left plots). The maximum energy error for Methods 2–5 without RE and for Methods 1–5 with RE is reached at  $t = T/2$ , the instant where the solution and its spatial derivative

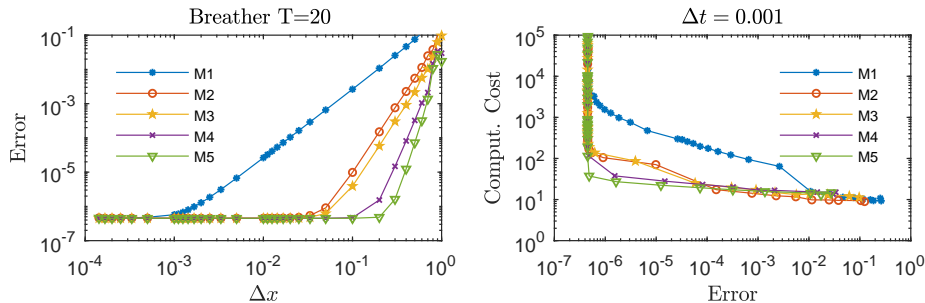


Figure 4: Numerical error (left plot) and computational cost (right plot) for the breather solution obtained with Methods 1–5 without Richardson extrapolation for  $T = 20$  and  $\Delta t = 1/1000$  as a function of  $\Delta x \in [1/7000, 1]$ .

becomes exactly null, but its time derivative has a local maximum; surprisingly, a careful evaluation indicates that the maximum error for Methods 2–5 with RE is equal to the addition of its result without RE plus that of Method 1. A comparison between the right plots in Fig. 2 with the left plots in Fig. 3 shows that the error in the discrete energy for  $\Delta t = 0.001$  and  $\Delta x = 0.01$  is dominated by the discretization in time; hence, the maximum error in the energy is exactly the same for Method 2–5 in the plots in both figures. Let us emphasize that the non-conservation of the discrete energy for Method 1 with RE results in a trend for the maximum error similar to that of the other methods, as shown in Fig. 3 (bottom left plot).

Figure 3 (right plots) shows the evolution in time of the speed of the kink (antikink) before (after) the collision in the kink-antikink solution. Since the speed  $v(t) = P(t)/E(t)$  of the exact kink-antikink solution is zero, the half-interval speed, defined as  $v_{1/2}(t) = 2 P_{1/2}(t)/E(t)$ , where  $P_{1/2}(t)$  is the half-momentum, has been used. The half-momentum is calculated by integrating Eq. (3) in the interval  $x \in (-\infty, 0)$ , and the discrete half-momentum by summing for  $m \in \{1, 2, \dots, M/2\}$  in Eq. (16). The half-interval speed for Methods 1–5 with and without RE are shown in Fig. 3 bottom right and top right plots, respectively. The curves are overlapped in both cases since all these methods approximately conserve the half-momentum with an error smaller than the resolution of the plot. Figure 3 (right plots) shows that, before the collision,  $v_{1/2}(t)$  is the speed of the kink,  $v_{1/2}(0) = 1/2$ , that decreases monotonically in time down to  $v_{1/2}(T/2) = 0$ ; after the collision,  $v_{1/2}(t)$  is negative, as expected for the speed of the antikink; as time passes it monotonically decreases from  $v_{1/2}(T/2) = 0$  down to  $v_{1/2}(T) = -1/2$ .

### 3.2. Breather

The breather solution for the sGE is given by

$$u_{br}(x, t) = 4 \tan^{-1} \frac{\sin(v(t-10)/r_+)}{\operatorname{sech}(x/r_+)/v},$$

310 where  $r_+ = \sqrt{1+v^2}$ , and  $v = 1/2$ . Let us take  $U_m^{-1} = u_{br}(x_m, -\Delta t)$ , and  $U_m^0 = u_{br}(x_m, 0)$ , as initial conditions for Methods 1–5. For the comparison among these methods, the numerical solution  $U_m^n$  for  $n = 2, 3, \dots, N$ , is calculated with  $T = 20$ ,  $L = 50$ , and  $\text{Tol}_{\text{rel}} = 10^{-14}$ .

315 Figure 4 (left plot) shows the numerical error  $\|U_m^N - u_{br}(x_m, 20)\|_\infty$  for Methods 1–5 without RE, with  $\Delta t = 1/1000$ , as a function of  $\Delta x \in \{1/7000, 1/6000, \dots, 1/1000, 1/900, 1/800, \dots, 1/100, 1/90, 1/80, \dots, 1/10, 2/10, 3/10, \dots, 1\}$ . For  $\Delta x \lesssim 0.001$  for Method 1,  $\Delta x \lesssim 0.05$  for Method 2 and 3,  $\Delta x \lesssim 0.1$  for Method 4, and  $\Delta x \lesssim 0.2$  for Method 5, the global error is dominated by error due to the discretization in time, reaching a constant value  $\approx 4.5 \times 10^{-7}$ ; as 320 expected, using values of  $\Delta t < 0.001$ , this plateau error can be reduced. Where the error due to the discretization in space dominates the global error, the high-order methods are more accurate than the lower order ones. Let us emphasize that Fig. 4 (left plot) shows results for  $\Delta x < \Delta t$ , violating the CFL condition, thanks to the unconditional stability of Methods 1–5. Figure 4 (right plot) 325 shows the run-time (in seconds) for Methods 1–5 without RE, with  $\Delta t = 0.001$  as a function of the numerical error. Method 2 is the most efficient one for errors larger than  $10^{-4}$ , but its cost is similar in magnitude to that of high-order methods; for errors smaller than  $10^{-4}$ , Method 5 is the most cost-effective one.

330 Figure 5 shows the numerical error  $\|U_m^N - u_{br}(x_m, 20)\|_\infty$  without (left plots) and with (right plots) RE for Methods 1 (first row) up to 5 (fifth row) for values of  $\Delta t \in \{0.001, 0.005, 0.01, 0.05, 0.1\}$ , as a function of  $\Delta x \in [0.001, 1]$ . Without RE, the error for Methods 1–5 (left plots) decreases until reaching a constant value, specifically, the error approaches  $0.44 \Delta t^2$ . These methods differ for large 335 enough  $\Delta x$ , being their slopes depending on the spatial order, as expected. With RE, the error of Methods 1–5 (right plots) decreases until reaching a constant value of about  $2.60 \Delta t^4$ ; but this behaviour can only be seen in the right plots for Method 1 with two largest values of  $\Delta t$ ; in fact, it cannot be seen for Methods 2–5 with  $\Delta t = 0.001$  for which the error oscillates randomly. 340 This oscillatory behaviour starts about  $\Delta x = 1/100$  for Methods 2–3, and about  $\Delta x = 1/60$  for Methods 4–5.

Table 2 shows the estimation of the spatial order for Methods 1–5 with and without RE by means of linear fitting of the logarithm for  $\Delta t = 0.001$  as a function of  $\Delta x$  large enough to avoid that the discretization in time dominates the

Table 2: The numerical order of accuracy in space of Methods 1–5 obtained by linear fitting of the logarithm of the error versus the logarithm of the grid size (fitted only for  $\Delta x$  such that the error in time is smaller than the error in space). The results in this table have  $L = 50$ ,  $\Delta t = 0.001$ , and  $T = 20$ .

	Method 1	Method 2	Method 3	Method 4	Method 5
Fit for $\Delta x \geq$	1/1000	1/20	1/20	1/9	1/8
Without RE	1.96	3.98	4.02	6.45	8.51
With RE	2.02	4.07	4.25	6.56	8.67

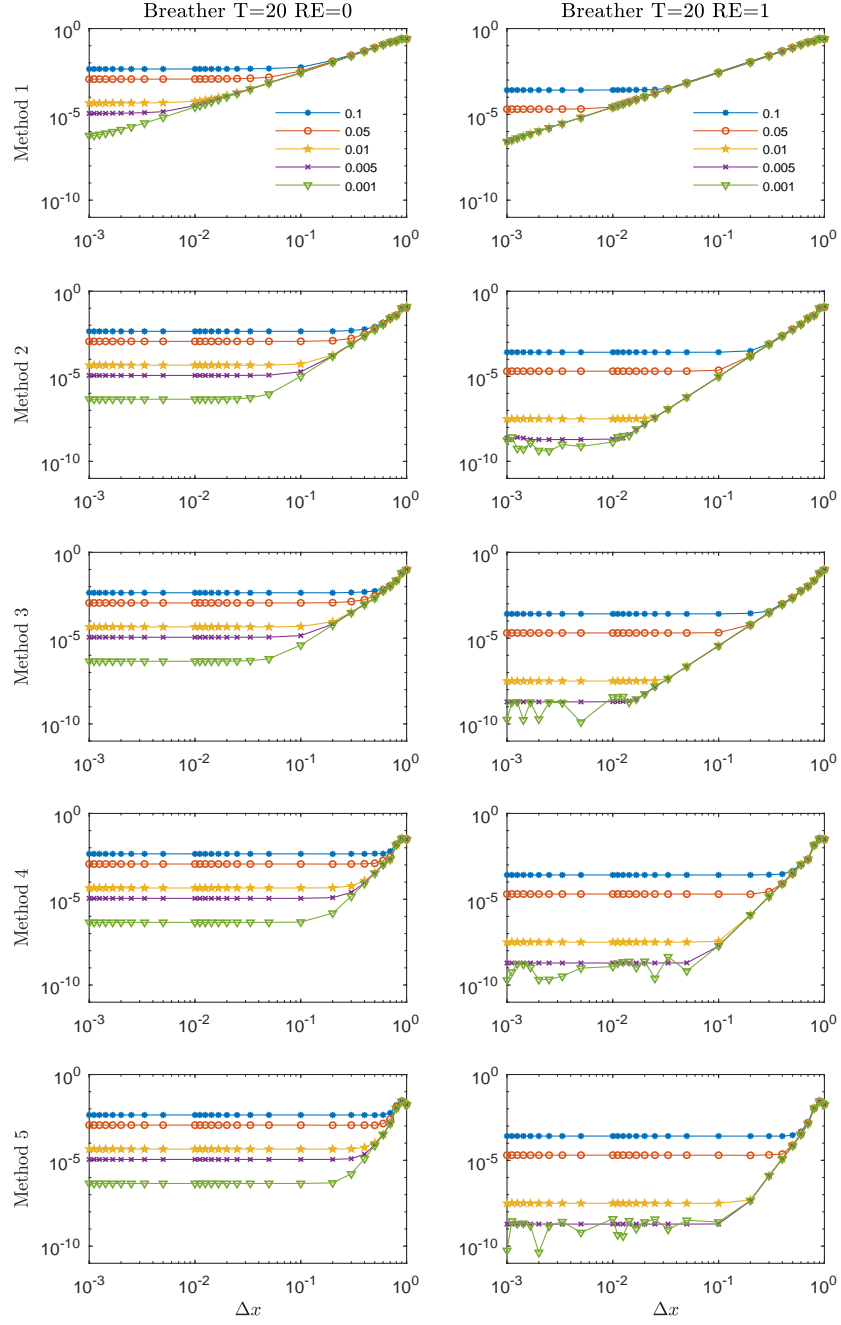


Figure 5: Numerical error without (left plots) and with (right plots) Richardson extrapolation for Methods 1–5 applied to the breather solution (3.2) with  $T = 20$  and  $L = 50$ , calculated with  $\Delta t \in \{0.001, 0.005, 0.01, 0.05, 0.1\}$  as a function of  $\Delta x \in [0.001, 1]$ .

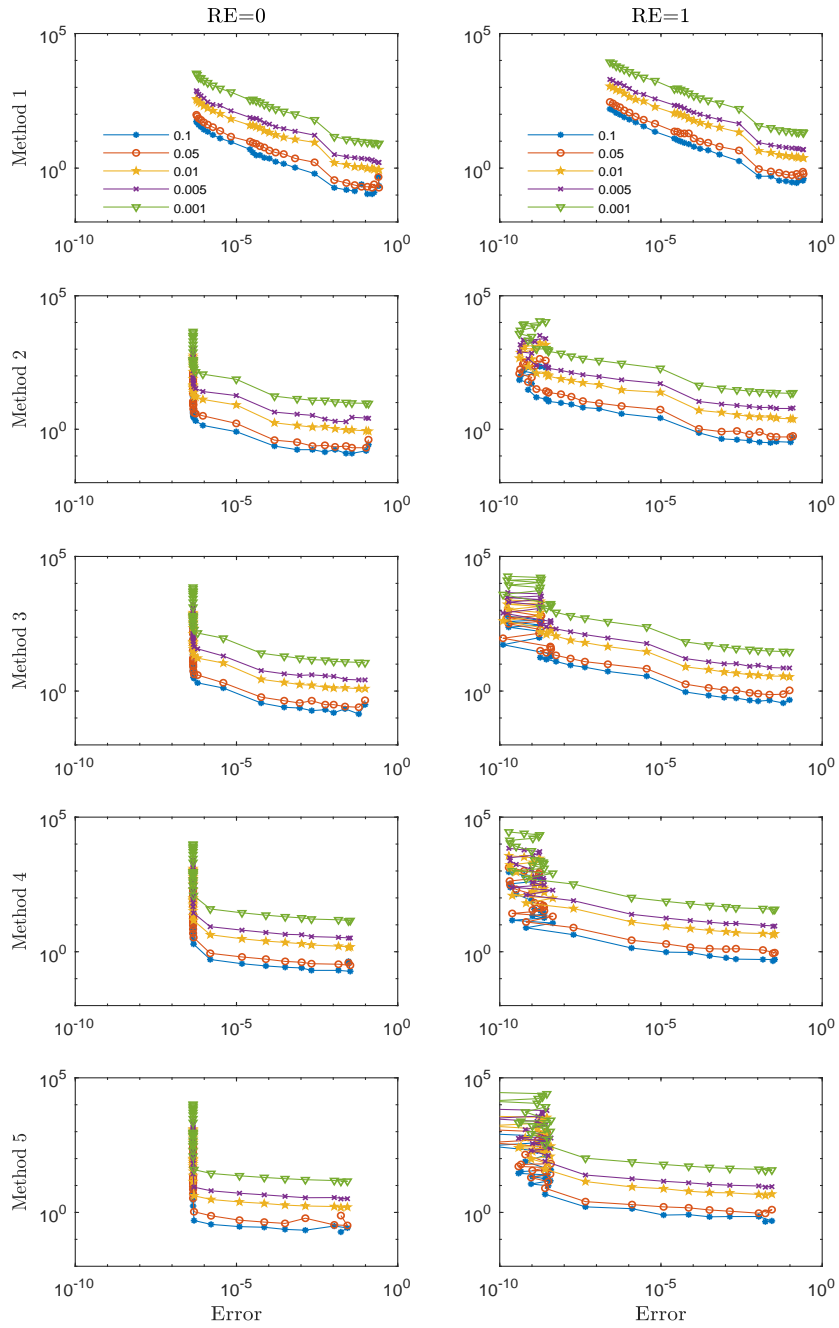


Figure 6: Computational costs (in seconds) without (left plots) and with (right plots) Richardson extrapolation for Methods 1–5 applied to the breather solution (3.2) with  $T = 20$  and  $L = 50$ , calculated with  $\Delta t \in \{0.001, 0.005, 0.01, 0.05, 0.1\}$  as a function of  $\Delta x \in [0.001, 1]$ .

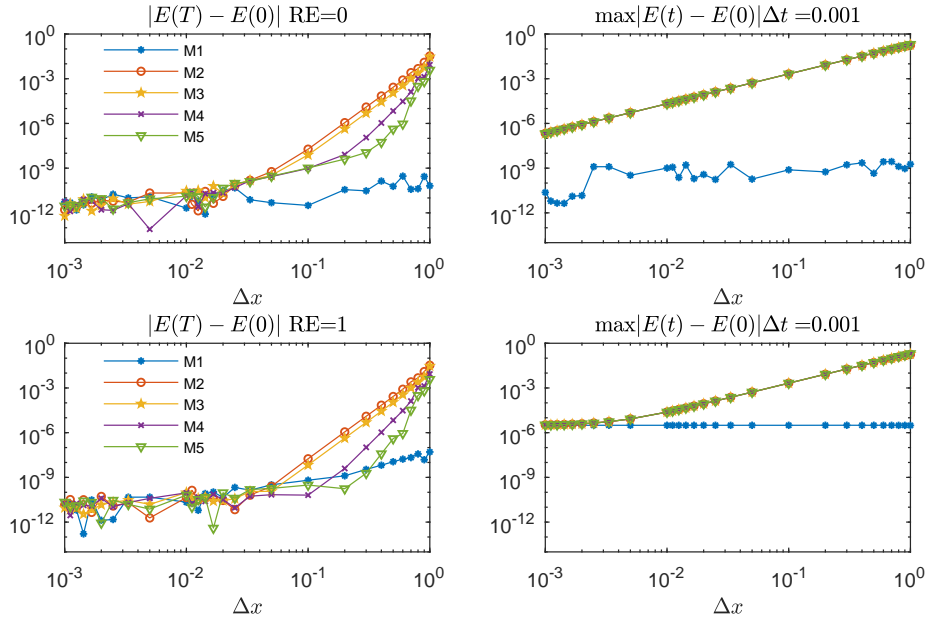


Figure 7: Numerical error of the discrete analogue of the energy (15) for the breather solution without (top plots) and with (bottom plots) Richardson extrapolation for  $T = 20$  and  $\Delta t = 0.001$  as a function of  $\Delta x \in \{1/1000, 1/900, 1/800, \dots, 1/100, 1/90, 1/80, \dots, 1/10, 2/10, 3/10, \dots, 1\}$ , for Methods 1–5. The left plots shows  $|E^N - E^0|$ , the numerical approximation of  $|E(T) - E(0)|$ , and right plots shows  $\|E^n - E^0\|_\infty$ .

345 global error (as seen in Fig. 5). As expected, the results are in good agreement with the theoretical orders of accuracy, cf. 2, 4, 4, 6, and 8, respectively.

Figure 6 shows the run-time (in seconds) for Methods 1 (first row) up to 5 (fifth row) with (right plots) and without (left plots) Richardson extrapolation for  $\Delta t \in \{0.001, 0.005, 0.01, 0.05, 0.1\}$  as a function of  $\Delta x \in [0.001, 1]$ . For all cases, the lowest cost is produced for the highest value of  $\Delta t$ . For errors larger than  $10^{-3}$ , Fig. 6 shows that Method 2 without RE is the most efficient method in terms of computational cost; for errors smaller than  $10^{-3}$ , the most cost-effective method is Method 5 with RE. As expected, from the kink–antikink numerical results, the most accurate method is the most cost-efficient one; note that Method 5 is tens of times more efficient than Method 1. Figure 6 (left plots) shows that without RE the smallest error attainable is about  $10^{-6}$ , but whenever RE is applied, as shown in Fig. 6 (right plots), the smallest error reachable is in the band of  $10^{-9}$  and  $10^{-10}$ .

360 Figure 7 illustrates the energy-conservation property of Methods 1–5 with (bottom plots) and without (top plots) RE; specifically, it shows the value of  $|E^N - E^0|$  (left plots) and  $\|E^n - E^0\|_\infty$  (right plots) with  $T = 20$  and  $\Delta t = 0.001$ , as a function of  $\Delta x \in [1/1000, 1]$ . Figure 7 (top left plot) shows that, as expected, Method 1 without RE conserves the discrete energy (15) for all  $\Delta x$ .

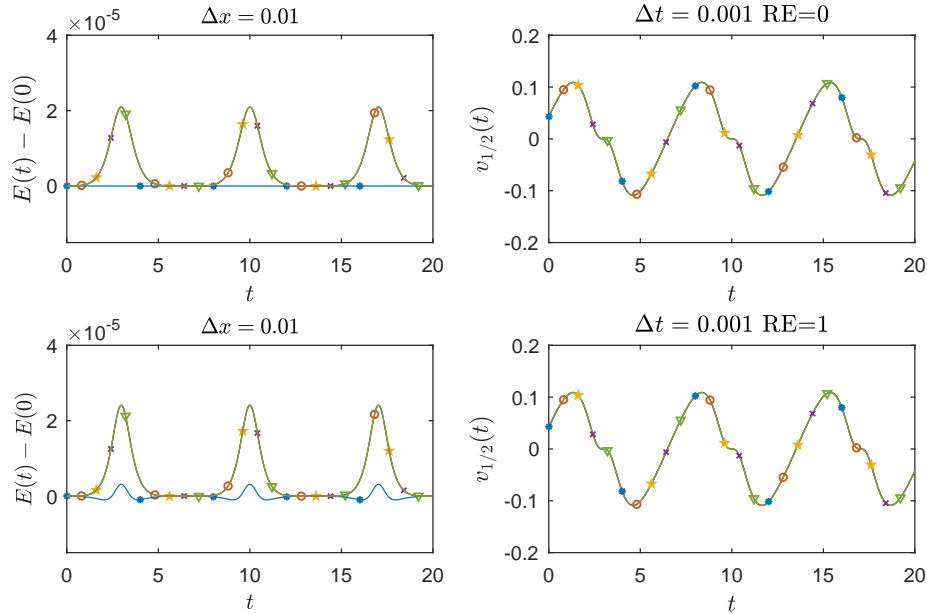


Figure 8: Numerical energy (left plots) and speed (right plots) of the breather solution with  $T = 20$ ,  $\Delta t = 0.001$ , and  $\Delta x = 0.01$ , for Methods 1–5 with (bottom plots) and without (top plots) Richardson extrapolation.

Methods 2–5 without RE only show good conservation properties for  $\Delta x \leq 1/30$ ;  
 365 however, for  $\Delta x > 1/30$  the error in the energy increases as the grid size does,  
 with a higher slope for higher-order methods. Figure 7 (bottom left plot) shows  
 that Method 1 with RE almost preserves the discrete energy; the loss of its  
 energy-conservation property was also observed with the kink–antikink solution  
 in Subsection 3.1. None of the Methods 2–5 with RE conserves the energy;  
 370 for  $\Delta x \leq 1/60$ , the maximum error coincides among all the methods, but for  
 $\Delta x > 1/60$  this error increases as the grid size does.

Figure 7 (top right plot) shows that the maximum error in the energy decreases  
 with  $\Delta x$  for Methods 2–5 without RE at the same rate, coinciding among  
 all of them; for Method 1 without RE the maximum error in the energy is very  
 375 small since it is conserved. Figure 7 (bottom right plot) shows that none of  
 the five methods with RE preserves the energy; for  $\Delta x \leq 1/300$ , the maximum  
 error coincides exactly among all the methods, but for  $\Delta x > 1/300$  this error  
 increases as the grid size does for Methods 2–5. For Method 1 with RE the  
 error reaches a constant value  $\approx 3.1 \times 10^{-6}$ .

380 Figure 8 (left plots) illustrates the maximum error in the discrete energy  
 in order to help the analysis of the results observed in Fig. 7 (right plots).  
 For Method 1 without RE the maximum error has a constant value, but for  
 Methods 2–5 without RE an oscillatory behaviour at the same frequency of the

breather solution is observed; due to the oscillation, it presents three maxima at  
 385  $t = 2.98, 10.0,$  and  $17.0,$  where the numerical energy reaches a maximum value  
 of  $2.095 \times 10^{-5}$  (top left plot). At these maxima, the breather solution and its  
 spatial derivative becomes null, hence the maximum error in the discrete energy  
 is dominated by the method of integration in time, which is exactly the same  
 for Method 2–5 without RE in Fig. 7 (right plots).

390 Figure 8 (right plots) shows the evolution in time of  $v_{1/2}(t),$  cf. Subsec-  
 tion 3.2, for the numerical breather solution. Methods 1–5 without RE, Fig. 8  
 (top right plot), and with RE, Fig. 8 (bottom right plot), the curves show the  
 same oscillatory behaviour for  $v_{1/2}(t),$  overlapping in the plots, since all these  
 methods approximately conserve the half-momentum with an error smaller than  
 395 the resolution of the plot, as in the case of the kink–antikink solution in Subsec-  
 tion 3.1. The value of  $v_{1/2}(t)$  oscillates at the same frequency that the breather,  
 with local maxima at  $t = 1.33, 8.36,$  and  $15.4,$  and local minima at  $t = 4.62,$   
 $11.6,$  and  $18.7$  for both with and without RE. Between the maxima and minima  
 there is a tiny plateau, at the same position of the maxima in Fig. 8 (left plot);  
 400 its origin is similar to the one observed in the kink-antikink case. In fact, as in  
 the kink-antikink case, the difference between the energy for Methods 2–5 with  
 RE (whose maximum value is  $2.41 \times 10^{-5}$ ) and that of Method 1 with RE (whose  
 maximum is  $3.13 \times 10^{-6}$ ) in Fig. 8 (bottom right plot) approximately coincides  
 with the energy for Methods 2–5 without RE (whose maximum is  $2.095 \times 10^{-5}$ )  
 405 in Fig. 8 (top right plot); in our opinion, the value for Method 1 is an estimation  
 of the contribution of the Richardson extrapolation to the non-conservation of  
 the energy in all the methods.

#### 4. Conclusions

Five numerical Padé schemes with and without Richardson extrapolation  
 410 for the sine-Gordon equation have been developed and analyzed. All of them  
 use the same second-order differences in time and the same approximation to  
 the nonlinearity, the one used by Guo Ben–Yu et al. [9]. Method 1 is a (0,2)-  
 Padé method conserving a discrete analog of the energy of the sGE and it is  
 of second-order in space; Method 2 is a (0,4)-Padé method which is fourth-  
 415 order accurate in space; Methods 3–5 are fourth-, sixth-, and eight-order order  
 (2,2)-, (2,4)-, and (4,4)-Padé methods, respectively. The local truncation error  
 terms of the five methods have been calculated by using Taylor series expan-  
 sion. Methods 1–5 are linearly, unconditionally stable. One level of Richardson  
 extrapolation have been used to increase the order of accuracy in time of the  
 420 numerical methods.

Methods 1–5 have been compared for both the kink–antikink and breather  
 solutions of the sGE obtaining similar results in both cases. The spatial order  
 of the methods has been validated by fitting the error for large enough  $\Delta x$   
 with respect to  $\Delta t,$  in order to avoid the contribution of the error due to the  
 425 discretization in time. The computational cost (the run-time in seconds) for  
 Methods 1–5 both with and without RE shows that Method 2 and 5 are the  
 most efficient one for errors larger than and smaller than  $10^{-3},$  respectively,

for the kink–antikink solution. For the breather solution, among Methods 1–5  
without RE is the most efficient one for errors larger than  $10^{-4}$  is Method 2, but  
430 for smaller ones is Method 5; moreover, Method 5 with RE is the most efficient  
one in all cases among Methods 1–5.

In the next future, there are several possibilities to be explored, like the  
use of diagonally implicit Runge–Kutta–Nyström methods, or the application  
of deferred correction techniques based on modified equations. Another fruitful  
435 line of further research is the application of our five numerical methods to the  
two-dimensional sine-Gordon equation [34], and to time-fractional and spatial-  
fractional sGE [35], including its extension to two dimensions [36].

### Acknowledgements

The research reported here was partially supported by Project DeepBIO  
440 (TIN2017-85727-C4-1-P) of the Programa Estatal de Fomento de la Investi-  
gación Científica y Técnica de Excelencia del Ministerio de Ciencia e Innovación  
of Spain.

### References

- [1] Barone A, Esposito F, Magee CJ, Scott AC. Theory and applica-  
445 tions of the sine-Gordon equation. Riv Nuovo Cimento 1971;1:227–67.  
<http://dx.doi.org/10.1007/BF02820622>.
- [2] Scott AC, Chu FYF, McLaughlin DW. The soliton: A new  
concept in applied science. Proc IEEE 1973;61(10):1443–83.  
<https://doi.org/10.1109/PROC.1973.9296>.
- 450 [3] Cuevas-Maraver J, Kevrekidis PG, Williams F. The sine-Gordon model  
and its applications. Nonlinear Systems and Complexity vol. 10; Berlin:  
Springer; 2014. <https://doi.org/10.1007/978-3-319-06722-3>.
- [4] Ablowitz MJ, Kaup DJ, Newell AC, Segur H. Method for solv-  
ing the Sine-Gordon equation. Phys Rev Lett 1973;30:1262–4.  
455 <http://dx.doi.org/10.1103/PhysRevLett.30.1262>.
- [5] Lamb Jr. GL. Elements of soliton theory. Pure & Applied Mathematics;  
New York: John Wiley & Sons; 1980.
- [6] Ablowitz MJ, Segur H. Solitons and the inverse scattering transform. SIAM  
460 studies in applied mathematics, vol. 4; Philadelphia: Society for Industrial  
and Applied Mathematics; 1981.
- [7] Ablowitz MJ, Clarkson PA. Solitons, nonlinear evolution equations and  
inverse scattering. London Mathematical Society Lecture Note Series vol.  
149; Cambridge: Cambridge University Press; 1991.

- [8] Martin-Vergara F, Rus F, Villatoro FR. Solitary waves on graphene superlattices. In: Archilla JFR, Palmero F, Lemos MC, Sánchez-Rey B, Casado-Pascual J, editors. *Nonlinear Systems, Vol. 2. Nonlinear Phenomena in Biology, Optics and Condensed Matter*. Berlin: Springer; 2018, p. 85–110. [https://doi.org/10.1007/978-3-319-72218-4\\_4](https://doi.org/10.1007/978-3-319-72218-4_4).  
465
- [9] Ben-Yu G, Pascual PJ, Rodriguez MJ, Vázquez L. Numerical solution of the sine-gordon equation. *Appl Math Comput* 1986;18(1):1–14. [https://doi.org/10.1016/0096-3003\(86\)90025-1](https://doi.org/10.1016/0096-3003(86)90025-1).  
470
- [10] Strauss W, Vázquez L. Numerical solution of a nonlinear Klein-Gordon equation. *J Comput Phys* 1978;28:271–8. [https://doi.org/10.1016/0021-9991\(78\)90038-4](https://doi.org/10.1016/0021-9991(78)90038-4).
- [11] Pascual PJ, Vázquez L. Sine-Gordon solitons under weak stochastic perturbations. *Physical Review B* 1985;32(12):8305–11. <https://doi.org/10.1103/PhysRevB.32.8305>.  
475
- [12] Bratsos AG, Twizell EH. The solution of the sine-Gordon equation using the method of lines. *Int J Comput Math* 1996;61(3–4):271–92. <https://doi.org/10.1080/00207169608804516>.  
480
- [13] Duncan D. Symplectic finite difference approximations of the nonlinear Klein-Gordon equation. *SIAM J Numer Anal* 1997;34(5):1742–60. <https://doi.org/10.1137/S0036142993243106>.
- [14] Bratsos AG. A numerical method for the one-dimensional sine-Gordon equation. *Numer Meth Part Differ Equ* 2008;24(3):833–44. <https://doi.org/10.1002/num.20292>.  
485
- [15] Sari M, Gürarlan G. A sixth-order compact finite difference method for the one-dimensional sine-Gordon equation. *Int J Numer Meth Biomed Eng* 2011;27(7):1126–38. <https://doi.org/10.1002/cnm.1349>.
- [16] Bratsos AG. A third order numerical scheme for the two-dimensional sine-Gordon equation. *Math Comput Simul* 2007;76(4):271–82. <https://doi.org/10.1016/j.matcom.2006.11.004>.  
490
- [17] Bratsos AG. The solution of the two-dimensional sine-Gordon equation using the method of lines. *J Comput Appl Math* 2007;206(1):251–77. <https://doi.org/10.1016/j.cam.2006.07.002>.  
495
- [18] Luo Y, Li X, Guo C. Fourth-order compact and energy conservative scheme for solving nonlinear Klein-Gordon equation. *Numer Meth Part Differ Equ* 2016;33(4):1283–304. <https://doi.org/10.1002/num.22143>.
- [19] Perring JK, Skyrme THR. A Model unified field equation. *Nucl Phys* 1962;31:550–5. [http://dx.doi.org/10.1016/0029-5582\(62\)90774-5](http://dx.doi.org/10.1016/0029-5582(62)90774-5).  
500

- [20] Martin-Vergara F, Rus F, Villatoro FR. Padé numerical schemes for the sine-Gordon equation. *App Math Comput* 2019; submitted.
- [21] Ablowitz MJ, Herbst BM, Schober CM. On the numerical solution of the sine-Gordon equation. *J Comput Phys* 1997;131(2):354–67. <https://doi.org/10.1006/jcph.1996.5606>.  
505
- [22] Wei GW. Discrete singular convolution for the sine-Gordon equation. *Physica D* 2000;137(3):247–59. [https://doi.org/10.1016/S0167-2789\(99\)00186-4](https://doi.org/10.1016/S0167-2789(99)00186-4).
- [23] Burg C, Erwin T. Application of Richardson extrapolation to the numerical solution of partial differential equations. *Numer Meth Part Differ Equ* 2009;25(4):810–32. <https://doi.org/10.1002/num.20375>.  
510
- [24] Djidjeli K, Price WG, Twizell EH. Numerical solutions of a damped sine-Gordon equation in two space variables. *J Eng Math* 1995;29(4):347–69. <https://doi.org/10.1007/BF00042761>.
- [25] Richards SA. Completed Richardson extrapolation in space and time. *Commun Numer Methods Eng* 1997;13(7):573–82. [10.1002/\(SICI\)1099-0887\(199707\)13:7<573::AID-CNM84>3.0.CO;2-6](https://doi.org/10.1002/(SICI)1099-0887(199707)13:7<573::AID-CNM84>3.0.CO;2-6).  
515
- [26] Deng D, Zhang C. A new fourth-order numerical algorithm for a class of nonlinear wave equations. *Appl Numer Math* 2012;62(12):1864–79. <https://doi.org/10.1016/j.apnum.2012.07.004>.  
520
- [27] Moghaderi H, Dehghan M. A multigrid compact finite difference method for solving the one-dimensional nonlinear sine-Gordon equation. *Math Meth Appl Sci* 2014;38(17):3901–22. <https://doi.org/10.1002/mma.3326>.
- [28] Lee J, Fornberg B. Some unconditionally stable time stepping methods for the 3D Maxwell’s equations. *J Comput Appl Math* 2004;166(2):497–523. <https://doi.org/10.1016/j.cam.2003.09.001>.  
525
- [29] Fornberg B, Zuev J, Lee J. Stability and accuracy of time-extrapolated ADI-FDTD methods for solving wave equations. *J Comput Appl Math* 2007;200(1):178–92. <https://doi.org/10.1016/j.cam.2005.12.012>.
- [30] Buckingham R, Miller PD. Exact solutions of semi-classical non-characteristic cauchy problems for the sine-gordon equation. *Physica D* 2008;237(18):2296–341. <https://doi.org/10.1016/j.physd.2008.02.010>.  
530
- [31] Vu-Quoc L, Li S. Finite difference calculus invariant structure of a class of algorithms for the nonlinear Klein-Gordon equation. *SIAM J Numer Anal* 1995;32(6):1839–75. <https://doi.org/10.1137/0732083>.  
535

- [32] Celledoni E, Grimm V, McLachlan RI, McLaren DI, O’Neale D, Owren B, et al. Preserving energy resp. dissipation in numerical PDEs using the “Average Vector Field” method. *J Comput Phys* 2012;231(20):6770–89. <https://doi.org/10.1016/j.jcp.2012.06.022>.  
540
- [33] Jiang C, Sun J, Li H, Wang Y. A fourth-order AVF method for the numerical integration of sine-Gordon equation. *App Math Comput* 2017;313:144–58. <https://doi.org/10.1016/j.amc.2017.05.055>.
- [34] Ameya D, Jagtap ASVM. Higher order scheme for two-dimensional inhomogeneous sine-Gordon equation with impulsive forcing. *Commun Nonlinear Sci Numer Simul* 2018;64:178–97. <https://doi.org/10.1016/j.cnsns.2018.04.012>.  
545
- [35] Macías-Díaz JE. Numerical study of the process of nonlinear supratransmission in Riesz space-fractional sine-Gordon equations. *Commun Nonlinear Sci Numer Simul* 2017;46:89–102. <https://doi.org/10.1016/j.cnsns.2016.11.002>.  
550
- [36] Zahra WK, Nasra MA. Exponentially fitted methods for solving two-dimensional time fractional damped Klein–Gordon equation with nonlinear source term. *Commun Nonlinear Sci Numer Simul* 2019;73:177–94. <https://doi.org/10.1016/j.cnsns.2019.01.016>.  
555